






Fabrication of spectrally sharp Si-based dielectric resonators: combining etaloning with Mie resonances

D. TOLIOPOULOS,^{1,2} M. KHOURY,^{1,6} M. BOUABDELLAOUI,^{1,6}  N. GRANCHI,^{3,6} J.-B. CLAUDE,^{1,4} A. BENALI,¹ I. BERBEZIER,¹ D. HANNANI,¹ A. RONDA,¹ J. WENGER,⁴ M. BOLLANI,⁵  M. GURIOLI,¹ S. SANGUINETTI,^{2,5} F. INTONTI,^{3,7} AND M. ABBARCHI^{1,8} 

¹Aix Marseille Univ, Université de Toulon, CNRS, IM2NP Marseille, France

²LNES and Department of Materials Science, University of Milano-Bicocca, via Cozzi 55, 20125 Milano, Italy

³LENS and Department of Physics and Astronomy, University of Florence, 50019 Sesto Fiorentino, Italy

⁴Aix Marseille Univ, CNRS, Centrale Marseille, Institut Fresnel, 13013 Marseille, France

⁵Istituto di Fotonica e Nanotecnologie-Consiglio Nazionale delle Ricerche, Laboratory for Nanostructure Epitaxy and Spintronics on Silicon, Via Anzani 42, 22100 Como, Italy

⁶These authors contributed equally to this work.

⁷intonti@lens.unifi.it

⁸marco.abbarchi@im2np.fr

Abstract: We use low-resolution optical lithography joined with solid state dewetting of crystalline, ultra-thin silicon on insulator (c-UT-SOI) to form monocrystalline, atomically smooth, silicon-based Mie resonators in well-controlled large periodic arrays. The dewetted islands have a typical size in the 100 nm range, about one order of magnitude smaller than the etching resolution. Exploiting a 2 μm thick SiO_2 layer separating the islands and the underlying bulk silicon wafer, we combine the resonant modes of the antennas with the etalon effect. This approach sets the resonance spectral position and improves the structural colorization and the contrast between scattering maxima and minima of individual resonant antennas. Our results demonstrate that templated dewetting enables the formation of defect-free, faceted islands that are much smaller than the nominal etching resolution and that an appropriate engineering of the substrate improves their scattering properties. These results are relevant to applications in spectral filtering, structural color and beam steering with all-dielectric photonic devices.

© 2020 Optical Society of America under the terms of the [OSA Open Access Publishing Agreement](#)

1. Introduction

Sub-micrometric, dielectric objects featuring high permittivity and reduced absorption losses enable for efficient light management, potentially enhancing and extending the performances of opto-electronic devices [1]. The resonant scattering supported by individual dielectric antennas is generally rather broad [2] (50-100 nm for the fundamental Mie resonances at visible and near-infrared frequency) and are strongly influenced by the coupling with the underlying substrate [3]. In addition, for individual resonators, the intensity contrast between maxima and minima is generally poor.

Common strategies for overcoming these limitations rely in coupling the nano-antennas together, forming complex oligomers and meta-surfaces, that can provide advanced functionalities and sharp resonances [1,4]. However, these approaches require for advanced fabrication methods to precisely set size, shape and relative position of the monomers (e.g. forming narrow gaps in between them). Another powerful approach, that has been recently used to improve the use

of dielectric Mie resonators as anti-reflection coatings, is the coupling of Fabry-Perot modes (formed within the effective medium containing Si-based nano-pillars) and Mie resonances (formed within the Si nano-pillars) in a single device [5].

Here we exploit the photonic modulation of the dielectric thick layers to extract more defined structural colors from dielectric Mie resonators. We fabricate monocrystalline Si-based islands via low-resolution optical lithography and plasma etching followed by solid state dewetting [6–12]. We show that the far-field scattering intensity of the Si-based islands sitting atop a 2 μm thick SiO_2 layer on bulk Si, can be efficiently coupled with etalon modes [3]. The Mie scattering efficiently out-couples the light interfering in the etalon according to the Si island size and re-directs the light at smaller angles with respect to the incident beam. From this combination spring structural colours covering the full visible spectrum and resonances with a high intensity contrast between maxima and minima. FDTD simulations account for this coupling showing that is a purely far-field effect with no modification of the local density of optical states (LDOS).

2. Methods

2.1. Fabrication

The mono-crystalline, ultra-thin, silicon on insulator (c-UT-SOI) is a single-crystal (001) film, 125 nm thick atop 2 μm thick SiO_2 layer (buried oxide, BOX) on a bulk Si (001) wafer (Fig. 1(a)). It is thinned to 20 nm SOI by rapid thermal oxidation (RTO) at 950 $^\circ\text{C}$ in O_2 atmosphere for 3 hours in order to transform the top part of the SOI in SiO_2 . By dipping the oxidised samples in a HF-solution at 5% in de-ionised water (95%) the top SiO_2 layer is removed thus exposing the remaining bottom SOI.

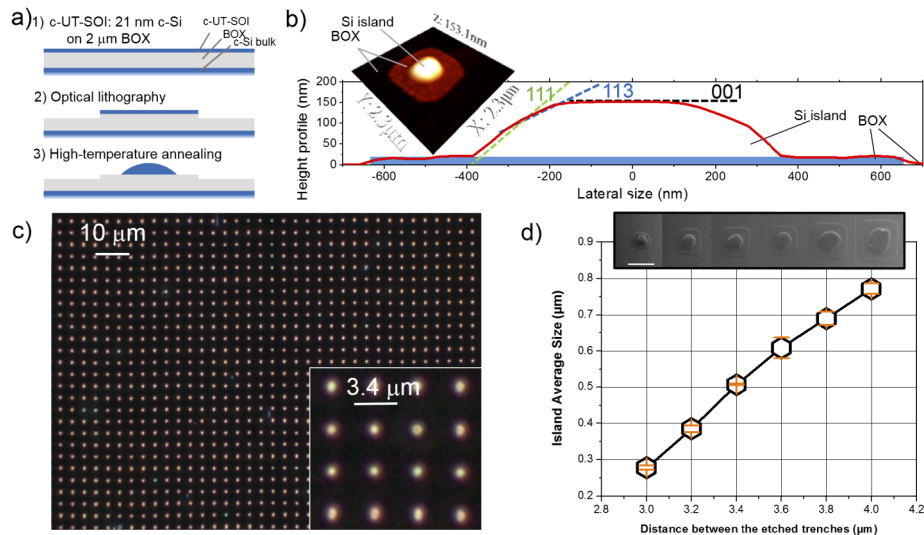


Fig. 1. a) Scheme of the main fabrication steps. 1) Crystalline, ultra-thin silicon on insulator (c-UT-SOI): 21 nm of monocrystalline Si (c-Si) on 2 μm of silicon oxide (buried oxide, BOX). 2) Optical lithography and plasma etching. 3) High temperature annealing in ultra-high vacuum. b) Atomic force microscope profile of an individual island. The main crystal facets are highlighted. The inset shows a 3D representation of the island. c) Optical dark-field image of a typical array of organized dewetted Si islands. The inset shows the homogeneity of the islands obtained with a periodicity of 3.4 μm . d) Average island size as a function between the etching pitch as obtained by scanning electron micrographs (SEM). The error bar represents the standard deviation. The line is a guide for the eyes. The top inset show a typical SEM for each etched pitch.

Island fabrication is performed in two steps: 1) patterning by photolithography and 2) solid state dewetting via high temperature annealing by following well established methods [9,11–13]. The photolithographic patterns are obtained by spin-coating a positive, photosensitive resist exposed to a near-UV laser (375 nm wavelength, fluency of about 2.7 mW) on a spot of about 2 μm (Dilase 250, from Kloe). The exposed portions of the resist are removed with a developer. Finally, a plasma etching step (70 seconds in CF_4 plasma, obtained in plasma-enhanced chemical vapor deposition machine from Oxford Instruments) attacks the exposed parts of the SOI, leaving intact the protected parts. By changing the pitch between vertical and horizontal lines (e.g. from 3 to 4 μm) we define squared patches having variable side (Fig. 1).

Before high-temperature annealing and dewetting the SOI are first chemically cleaned with acetone, ethanol, O_2 plasma and finally in a HF solution at 5% in de-ionised water under N_2 atmosphere in a glove box. The SOI samples are transferred to the ultra-high vacuum ($\sim 10^{-10}$ torr) of the molecular beam epitaxy chamber (MBE) (RIBER 32 MBE system). The annealing process is carried out in two stages, the first one is an *in-situ* cleaning where the temperature is risen at about 650 $^\circ\text{C}$ for 30 minutes in order to remove any residual native oxide from the surface of the sample. The second annealing step induces the solid-state dewetting of the SOI when the temperature is increased at about 750 $^\circ\text{C}$ for 30 minutes.

2.2. Characterization

Dark field (DF) images and spectra were collected by using an optical microscope (ZEISS Axio Observer) mounting a 100X magnification objective lens (numerical aperture $\text{NA} = 0.9$) working both in bright and dark field configurations, coupled with a spectrometer and Si-based CCD linear array (Flame-T-VIS-NIR by Ocean Optics). In order to investigate individual islands, the scattered light was collected using an optical fiber (Ocean Optics multimode fiber, VIS-NIR, core diameter 200 μm) defining a lateral resolution of about 2 μm .

The Si islands were imaged via scanning electron microscopy (SEM) performed with a FEI Helios 600 Nano-Lab. Micrographs were acquired using a secondary electron through-the-lens detector (5 kV acceleration voltage), probe current of 0.17 nA and working distance of 4.2 mm. Atomic force microscopy (XE-100 AFM from Park systems) was performed in non-contact mode.

2.3. Simulations

To clarify the influence of the 2 μm thick BOX layer on the island scattering spectra, numerical calculations were performed with a commercial three-dimensional 3D finite-difference time domain (FDTD) code (CrystalWave, Photon Design). We consider a hemispherical Si island with 200 nm base diameter and a refractive index $n = 4$, neglecting absorption. The Si island is excited with a broadband point-like dipole (emitting at $\lambda = 600$ nm, with a full width at half maximum $\text{FWHM} = 300$ nm) positioned in the middle of the island, with polarization parallel to the BOX surface. The flux of the Poynting vector across a box sensor, a cube of side 300 nm, positioned around the exciting dipole gives us the LDOS of the island at the dipole position [14].

3. Results

3.1. Templated dewetting of Si-based Mie resonators on thick BOX

At the end of the dewetting process we obtain monocrystalline and atomically smooth islands featuring the typical facets of the equilibrium shape of silicon (Fig. 1(b)) [7–10,12,15]. Large islands arrays (Fig. 1(c)) can be fabricated with controlled size (base diameter from about 280 to 780 nm) and regular organization [8,11,15,16] (Fig. 1(d)). The similar scattering color accounts for a good homogeneity, as also confirmed by the small fluctuation obtained by measuring the base size of several islands for each pitch (error bars in Fig. 1(d)). Islands height are in the 90 to 150 nm range, depending on the initial pitch size (see an example of large island in the AFM

image in Fig. 1(b)). Smaller island size (e.g. featuring bright scattering at visible frequency) can be obtained by reducing the pitch of the lithographic step [8,11,15,16] (not shown).

3.2. Dark-field spectroscopy of individual Mie resonators

For optical spectroscopy at visible frequency (owing to the limits of our silicon-based detector) we chose a set of dewetted islands with increasing base diameter, from about 100 to 200 nm (Fig. 2(a)), left column) [8,9,11,15]. Slight shape asymmetries observed in some island are ascribed to a non-complete dewetting that did not lead to the final equilibrium shape of silicon crystals. In principle, these defects could be improved with a longer annealing time or a higher temperature.

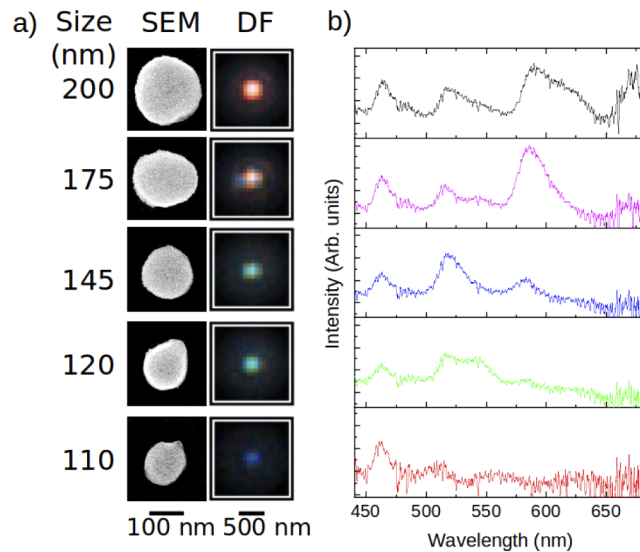


Fig. 2. a) Left column: SEM images of crystalline Si dewetted islands. Their corresponding size is highlighted at their left. Right panel: dark-field optical microscope images of the islands shown in the left column. b) Dark-field scattering spectrum corresponding to the islands shown in a). Further characterization of the color scattered by these islands is reported in [Supplement 1](#).

Dark field images reveal a net colorization from blue to red, when increasing particle size (Fig. 2(a)), right column). The corresponding scattering spectra (normalised by the white lamp used for illumination) confirm this tendency, showing several sharp bands that increase in number at long wavelength for larger islands (Fig. 2(b)) [9,11]. These resonances share a similar spectral position and spacing between them, although some differences (up to 25-30 nm) are observed (see also Fig. 2) [3]. These differences can be accounted for by imperfections in the etching (locally thicker or thinner BOX), incomplete dewetting leaving some pristine c-UT-SOI nearby the islands, residual Si particles on the BOX nearby the islands, intermixing of Si and SiO₂ [17–19], and asymmetries in the dewetted islands [9].

3.3. Comparison with etalon reflection

In order to confirm that the observed far field spectra are due to strong spectral variations of the driving field in the resonators related with constructive and destructive interference of the incident light at the air-SiO₂ and SiO₂-Si interfaces, we simulate the specular reflection from a bare 2 μm thick, flat SiO₂ layer atop bulk Si (that mimics the BOX underneath the dewetted islands, Fig. 3(a)). These simulations were compared with the dark field scattering spectrum of a large

silicon island, Fig. 3(b)). The specular reflection at normal incidence (0 degrees) features 5 broad peaks in the investigated spectral range having a contrast of about 3 (Fig. 3(a) top panel). For 70 degrees incidence (that is similar to the incidence angle of the light in dark-field configuration) the overall picture is similar but the peaks are only four, with a pronounced flattening at their top and with a lower contrast of roughly 2 (Fig. 3(a) bottom panel). These latter features are understood by observing the *s* and *p* polarized components of the reflection: they present maxima and minima in opposition of phase thus providing a more complex behavior with respect to the normal incidence case, where the two components are identical. Note that at this large incident angle, the *s* polarization is dominant with an intensity that is about double with respect to that one of the *p* counterpart.

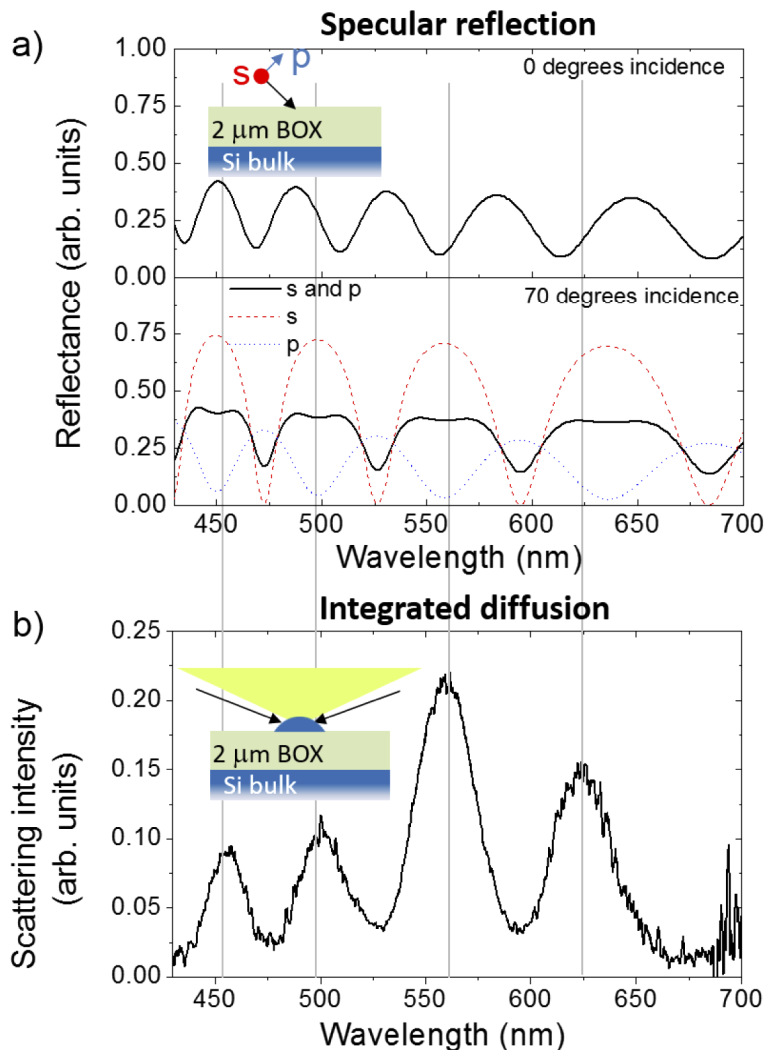


Fig. 3. a) Simulated intensity of the specular reflection for *s* and *p* polarization from a 2 μm thick SiO_2 layer (BOX) atop Si bulk. Top panel: normal incidence. Bottom panel: 70 degrees incidence. The inset highlights the geometry considered in the model. b) Dark-field scattering spectrum of a dewetted island. The inset highlights excitation and collection conditions (respectively ~ 70 degrees incidence and within a 64 degrees aperture cone).

The scattering spectrum of the individual Si island shows 4 peaks with a rather large intensity contrast (between 3 and 6, depending on the peak taken into account, Fig. 3(b)). The spectral position and spacing between the scattering peaks show marked similarities with the reflection spectrum of the flat SiO₂ layer when comparing the case of *s* polarization at an incidence of 70 degrees (as highlighted by the vertical gray lines in (Fig. 3). Moreover, also the broadening of the resonances observed in the scattering spectrum and in the *s* polarised reflection are rather similar: they show an increasing trend from about 25 nm for the shorter wavelength resonance up to 35 nm for the longer wavelength one. This broadening of the resonant scattering is 4 to 3 times smaller than what was reported for similar Si islands formed via solid state dewetting atop a 145 nm thick BOX [9], where the etaloning effect is negligible [3].

4. Discussion

The use of solid state dewetting for the fabrication of ordered and disordered dielectric Mie resonators made of Si(Ge) has been largely addressed in the past years. [9–11,20–22] However, obtaining ordered arrays of simple islands or complex nano-architectures required so far, e-beam lithography and reactive etching [4,23] or direct etching via focused ion beam [8,11,13,16]. Although very precise, these methods are rather costly and eventually difficult to extend to very large surfaces. Here we replaced these approaches extending the idea of templated dewetting to conventional optical lithography. This is a much less expensive technique and can, in principle, be extended to larger areas. In our case the lateral etching resolution was rather poor, only 2 μm . Although this does not allow for a large islands density (the minimal distance between island is about 2 μm), it is worth noting that large homogeneous arrays of nano-objects can be obtained. This is possible thanks to the dewetting approach, that leads to the collapse of all the c-UT-SOI present in the original patch in a single island, thus effectively gaining a factor of the order of 10 in lateral resolution [12]. These islands can be organized in large arrays with a fine size tuning and a small spread in size (size distribution is within 10% or smaller). This size distribution is improved with respect to previous reports of Si and SiGe templated-dewetting where the etching was performed with a focused ion beam [8,11,13,16] and are similar to those reported for e-beam lithography and reactive ion etching [10,12].

Aside, we also note that the use of this self-assembly method enables the formation of monocrystalline objects with atomically smooth, faceted interfaces [7–9,12,15,21]. A feature that cannot be obtained with other conventional top-down methods that always induce a more or less pronounced roughness and it may be an advantage when electronic properties are concerned [12].

Let's move to the discussion of the optical properties. **Combining the sharper resonances springing from the etalon effect produced by the thick BOX atop the Si bulk and the broader Mie scattering (see also Fig. 2) we obtain colours that are qualitatively similar to those obtained with in state-of-the-art SiGe- [11] and Si-based [23] Mie resonators** (respectively obtained via templated dewetting and e-beam lithography and reactive ion etching). Provided the hybrid top-down/bottom-up approach in use, our resonators are not scattered and mixed in size as for purely bottom-up methods [24,25] and can be organized in large and regular arrays featuring a small size dispersion. For a quantitative characterization of the color see [Supplement 1](#).

The scattering data, linked to the reflection simulation of the silica etalon, lead to the conclusion that the *s* polarization is playing a major role in the observed structural color. In addition to the more intense *s* polarization excitation associated to the etalon effect (Fig. 3(a) bottom panel), we expect less scattering around normal incidence for *p* polarization due to the electric dipole angular pattern [3]. Indeed, a marked similarity emerges when observing the spectrum of the *s* polarised specular reflection at 70 degrees of incidence (Fig. 3(a) bottom panel) and the dark-field resonant scattering spectrum of the Si island (Fig. 3(b)). This suggests that the Mie resonator back scatters some of the incident light reflected at the air-SiO₂ and SiO₂-Si interfaces. Note that, in the geometry of the dark-field experiment, the direct reflection of the incident beam (at about 70

degrees) is not detected. In fact, the areas nearby the islands are dark, as the numerical aperture of the detection is only 64 degrees. Thus, the resonant scattering redirects the reflected light at different angles with respect to the incident ones while preserving some of the features of the interference in the etalon.

In order to corroborate the picture that the scattering spectrum of the islands is strongly influenced by interference effects and is not due to a modification of the LDOS of the Si island, we compare the FDTD simulation of an hemispherical Si island placed atop of 2 μm thick layer of SiO_2 ($n = 1.5$) plus a 1 μm thick substrate of Si ($n = 4$) with the same island atop only 2 μm of SiO_2 (Fig. 4).

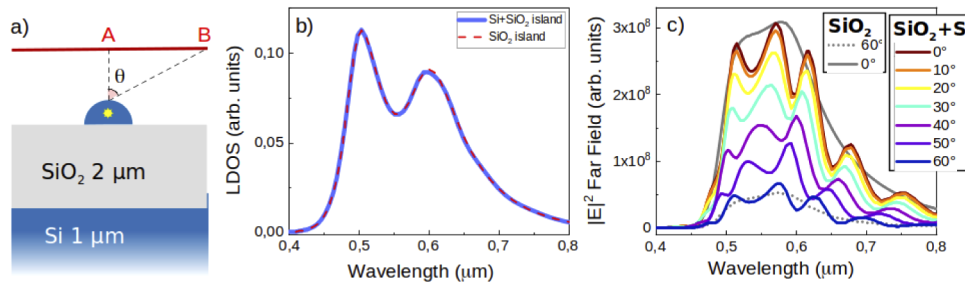


Fig. 4. a) Sketch of the simulated structure: a hemispherical Si island on a substrate formed by a 2 μm SiO_2 layer atop 1 μm Si layer. The yellow star, in the middle of the island, represents the broadband point-like dipole (emitting with a central wavelength of 600 nm, with a full width at half maximum FWHM = 300 nm) that acts as excitation source. The red line indicates the far field sensor, positioned at a height such that the points A and B correspond to an acquisition angle θ of 0 degrees and 60 degrees, respectively. b) Local Density of States (LDOS) of the island sitting atop 2 μm SiO_2 layer only (red dashed line) and on 2 μm SiO_2 plus 1 μm Si (blue line). c) Colored lines: far field simulated spectra acquired at different values of theta for the island atop 2 μm SiO_2 plus 1 μm Si substrate (from $\theta = 0$ to 60 degrees). The far field intensity from the island on 2 μm SiO_2 layer only, are represented for comparison in the two limit cases $\theta = 0$ and 60 degrees) in grey (respectively continuous and dashed lines).

Parallel to the BOX surface, at a distance of 1 μm is positioned a planar sensor, that allows to simulate the collected far field spectra under different acquisition angles, reported in Fig. 4(c)). The simulations conditions are different with respect to the experimental ones and their aim is to explain the underlying phenomenology. A quantitative comparison with the experimental data goes beyond the aim of this paper.

The LDOS spectra (Fig. 4(b)) are calculated at the position of the exciting dipole by following Ref. [14] and are dominated by two resonances at about 500 nm and 600 nm, that can be identified as the electric (ED) and magnetic dipolar (MD) modes, respectively [3,9,11,20]. The two curves, within the line thickness, are identical, giving an indication that the LDOS of the Si-island is not significantly modified by the presence of the Si substrate. On the contrary, the far field spectra are dramatically influenced by the presence of the Si substrate. Far-field spectra collected at different points of the far field sensor correspond to spectra detected at different acquisition angles (Fig. 4(c)). The simulation without the Si substrate shows smooth spectra (solid and dashed gray lines) where is possible to identify the ED and MD modes characterized by different relative weights. The scattering intensity at 0 degrees is about six times more intense with respect to that one at 60 degrees. The far field spectra obtained by taking into account the Si substrate show a clear intensity modulation superimposed on the smooth spectra obtained without Si substrate. The spectral position of the observed fringes shifts toward the blue by increasing the detection angle. A similar effect is observed by considering the specular reflection of 2 μm

of SiO₂ on Si (not shown). This study clearly confirms that the modulations observed in the far-field scattering intensity are not related to a modification of the LDOS of the Si islands. They are rather related to the scattering by the Mie resonator of the incident light beam propagating and interfering in the SiO₂ layer sandwiched between the island and the bulk Si substrate.

5. Conclusion

In conclusion we showed that a low resolution etching method joined with solid-state dewetting can provide ordered arrays of monocrystalline Si-based islands with size control and featuring a bright Mie scattering in the visible spectral range. Coupling the scattering with etalon resonances allows to fix the position of maxima and minima and enhance the contrast between them with respect to individual dielectric antennas. In addition to this, our simple approach enables to obtain good structural colours avoiding the use of expensive and slow fabrication tools.

Our design has relevant features in terms of dielectric antennas for quantum emitters [26–28]. The simulation indicates a spectral dependent emission steering of the Mie antenna when coupled with the dielectric etalon. This effect can be exploited for quantum applications, such as the selective and different directionality in exciton-biexciton cascade of a quantum emitter [29] embedded in Mie resonators.

Funding

H2020 European Research Council (721394, 828890); European Research Council (723241); Agence Nationale de la Recherche (ANR-15-CE24-0027-01, ANR-18-CE47-0013-03).

Acknowledgments

We acknowledge the NanoTecMat platform of the IM2NP institute of Marseille. This research was funded by the EU H2020 FET-OPEN project NARCISO (ID: 828890). J.W. and J-B. C. acknowledge the European Research Council (ERC, grant agreement No 723241). A.B. and M.A. acknowledge the PRCI network ULYSSES (ANR-15-CE24-0027-01). M.K. and M.A. acknowledge the ANR project OCTOPUS (ANR-18-CE47-0013-03), D.T. and S.S acknowledge funding from EU H2020 MSCA project 4PHOTON (ID: 721394).

Disclosures

The authors declare no conflicts of interest.

See [Supplement 1](#) for supporting content.

References

1. T. Liu, R. Xu, P. Yu, Z. Wang, and J. Takahara, "Multipole and multimode engineering in mie resonance-based metastructures," *Nanophotonics* **9**(5), 1115–1137 (2020).
2. T. Coenen, J. van de Groep, and A. Polman, "Resonant modes of single silicon nanocavities excited by electron irradiation," *ACS Nano* **7**(2), 1689–1698 (2013).
3. J. Van de Groep and A. Polman, "Designing dielectric resonators on substrates: Combining magnetic and electric resonances," *Opt. Express* **21**(22), 26285–26302 (2013).
4. Y. Yang, I. I. Kravchenko, D. P. Briggs, and J. Valentine, "All-dielectric metasurface analogue of electromagnetically induced transparency," *Nat. Commun.* **5**(1), 5753–5757 (2014).
5. A. Cordaro, J. Van De Groep, S. Raza, E. F. Pecora, F. Priolo, and M. L. Brongersma, "Antireflection high-index metasurfaces combining mie and fabry-perot resonances," *ACS Photonics* **6**(2), 453–459 (2019).
6. C. V. Thompson, "Solid-State Dewetting of Thin Films," *Annu. Rev. Mater. Res.* **42**(1), 399–434 (2012).
7. M. Aouassa, L. Favre, A. Ronda, H. Maaref, and I. Berbezier, "The kinetics of dewetting ultra-thin si layers from silicon dioxide," *New J. Phys.* **14**(6), 063038 (2012).

8. M. Aouassa, I. Berbezier, L. Favre, A. Ronda, M. Bollani, R. Sordan, A. Delobbe, and P. Sudraud, "Design of free patterns of nanocrystals with ad hoc features via templated dewetting," *Appl. Phys. Lett.* **101**(1), 013117 (2012).
9. M. Abbarchi, M. Naffouti, B. Vial, A. Benkouider, L. Lermusiaux, L. Favre, A. Ronda, S. Bidault, I. Berbezier, and N. Bonod, "Wafer scale formation of monocrystalline silicon-based mie resonators via silicon-on-insulator dewetting," *ACS Nano* **8**(11), 11181–11190 (2014).
10. M. Naffouti, R. Backofen, M. Salvalaglio, T. Bottein, M. Lodari, A. Voigt, T. David, A. Benkouider, I. Fraj, L. Favre, A. Ronda, I. Berbezier, D. Grosso, M. Abbarchi, and M. Bollani, "Complex dewetting scenarios of ultrathin silicon films for large-scale nanoarchitectures," *Sci. Adv.* **3**(11), ea01472 (2017).
11. T. Wood, M. Naffouti, J. Berthelot, T. David, J.-B. Claude, L. Métayer, A. Delobbe, L. Favre, A. Ronda, I. Berbezier, N. Bonod, and M. Abbarchi, "All-dielectric color filters using SiGe-based mie resonator arrays," *ACS Photonics* **4**(4), 873–883 (2017).
12. M. Bollani, M. Salvalaglio, A. Benali, M. Bouabdellaoui, M. Naffouti, M. Lodari, S. Di Corato, A. Fedorov, A. Voigt, I. Fraj, L. Favre, J. B. Claude, D. Grosso, G. Nicotra, A. Mio, A. Ronda, I. Berbezier, and M. Abbarchi, "Templated dewetting of single-crystal, ultra-long nano-wires and on-chip silicon circuits," *Nat. Commun.* **10**(1), 5632 (2019).
13. M. Naffouti, T. David, A. Benkouider, L. Favre, A. Ronda, I. Berbezier, S. Bidault, N. Bonod, and M. Abbarchi, "Fabrication of poly-crystalline si-based mie resonators via amorphous si on sio 2 dewetting," *Nanoscale* **8**(14), 7768 (2016).
14. D. Pellegrino, D. Balestri, N. Granchi, M. Ciardi, F. Intonti, F. Pagliano, A. Y. Silov, F. W. Otten, T. Wu, K. Vynck, P. Lalanne, A. Fiore, and M. Gurioli, "Non-lorentzian local density of states in coupled photonic crystal cavities probed by near-and far-field emission," *Phys. Rev. Lett.* **124**(12), 123902 (2020).
15. I. Berbezier, M. Aouassa, A. Ronda, L. Favre, M. Bollani, R. Sordan, A. Delobbe, and P. Sudraud, "Ordered arrays of si and ge nanocrystals via dewetting of pre-patterned thin films," *J. Appl. Phys.* **113**(6), 064908 (2013).
16. M. Naffouti, T. David, A. Benkouider, L. Favre, A. Delobbe, A. Ronda, I. Berbezier, and M. Abbarchi, "Templated solid-state dewetting of thin silicon films," *Small* **12**(44), 6115–6123 (2016).
17. F. Leroy, Y. Saito, S. Curio, F. Cheynis, O. Pierre-Louis, and P. Müller, "Shape transition in nano-pits after solid-phase etching of sio2 by si islands," *Appl. Phys. Lett.* **106**(19), 191601 (2015).
18. F. Leroy, T. Passanante, F. Cheynis, S. Curio, E. Bussmann, and P. Müller, "Catalytically enhanced thermal decomposition of chemically grown silicon oxide layers on si (001)," *Appl. Phys. Lett.* **108**(11), 111601 (2016).
19. M. Trautmann, F. Cheynis, F. Leroy, S. Curio, and P. Müller, "Interplay between deoxidation and dewetting for ultrathin soi films," *Appl. Phys. Lett.* **110**(16), 161601 (2017).
20. M. Bouabdellaoui, S. Checcucci, T. Wood, M. Naffouti, R. P. Sena, K. Liu, C. M. Ruiz, D. Duche, J. Le Rouzo, L. Escoubas, G. Berginc, N. Bonod, M. Zazoui, L. Favre, L. Metayer, A. Ronda, I. Berbezier, D. Grosso, M. Gurioli, and M. Abbarchi, "Self-assembled antireflection coatings for light trapping based on siige random metasurfaces," *Phys. Rev. Mater.* **2**(3), 035203 (2018).
21. M. Naffouti, M. Salvalaglio, T. David, J.-B. Claude, M. Bollani, A. Voigt, A. Benkouider, L. Favre, A. Ronda, I. Berbezier, A. Delobbe, A. Houel, and M. Abbarchi, "Deterministic three-dimensional self-assembly of si through a rimless and topology-preserving dewetting regime," *Phys. Rev. Mater.* **3**(10), 103402 (2019).
22. M. Salvalaglio, M. Bouabdellaoui, M. Bollani, A. Benali, L. Favre, J.-B. Claude, J. Wenger, P. de Anna, F. Intonti, A. Voigt, and M. Abbarchi, "Hyperuniform monocrystalline structures by spinodal solid-state dewetting," *Phys. Rev. Lett.* **125**(12), 126101 (2020).
23. V. Flauraud, M. Reyes, R. Paniagua-Dominguez, A. I. Kuznetsov, and J. Brugger, "Silicon nanostructures for bright field full color prints," *ACS Photonics* **4**(8), 1913–1919 (2017).
24. W. Chaabani, J. Proust, A. Movsesyan, J. Beal, A.-L. Baudrion, P.-M. Adam, A. Chehaidar, and J. Plain, "Large-scale and low-cost fabrication of silicon mie resonators," *ACS Nano* **13**(4), 4199–4208 (2019).
25. A. Benali, J.-B. Claude, N. Granchi, S. Checcucci, M. Bouabdellaoui, M. Zazoui, M. Bollani, M. Salvalaglio, J. Wenger, L. Favre, D. Grosso, A. Ronda, I. Berbezier, M. Gurioli, and M. Abbarchi, "Flexible photonic devices based on dielectric antennas," *JPhys Photonics* **2**(1), 015002 (2020).
26. B. Rolly, B. Stout, and N. Bonod, "Boosting the directivity of optical antennas with magnetic and electric dipolar resonant particles," *Opt. Express* **20**(18), 20376–20386 (2012).
27. R. Regmi, J. Berthelot, P. M. Winkler, M. Mivelle, J. Proust, F. Bedu, I. Ozerov, T. Begou, J. Lumeau, H. Rigneault, M. F. García-Parajó, S. Bidault, J. Wenger, and N. Bonod, "All-dielectric silicon nanogap antennas to enhance the fluorescence of single molecules," *Nano Lett.* **16**(8), 5143–5151 (2016).
28. I. Suarez, T. Wood, J. P. M. Pastor, D. Balestri, S. Checcucci, T. David, L. Favre, J. B. Claude, D. Grosso, A. F. Gualdrón-Reyes, M. Abbarchi, and M. Gurioli, "Enhanced nanoscopy of individual cspbbr3 perovskite nanocrystals using dielectric sub-micrometric antennas," *APL Mater.* **8**(2), 021109 (2020).
29. N. Dotti, F. Sarti, S. Bietti, A. Azarov, A. Kuznetsov, F. Biccari, A. Vinattieri, S. Sanguinetti, M. Abbarchi, and M. Gurioli, "Germanium-based quantum emitters towards a time-reordering entanglement scheme with degenerate exciton and biexciton states," *Phys. Rev. B* **91**(20), 205316 (2015).